Cationic metal-organic framework with charge separation effect as a high output triboelectric nanogenerator material for self-powered anticorrosion

Zhichao Shao,*[a] Haoran Cheng,[a] Yi Wei,[b] Junshuai Chen,[a] Kexin Gao,[a] Zhe Fang,[a] Yangshuang Yan,[a] Liwei Mi*[a] and Hongwei Hou*[b]

[a] Center for Advanced Materials Research, Zhongyuan University of Technology, Zhengzhou, 450007, P. R. China.

[b] College of Chemistry, Zhengzhou University, Zhengzhou, Henan, 450001, P. R. China.

E-mail address: *shaozhichao@zut.edu.cn*, *mlwzzu@163.com*, *houhongw@zzu.edu.cn*

Supporting Information

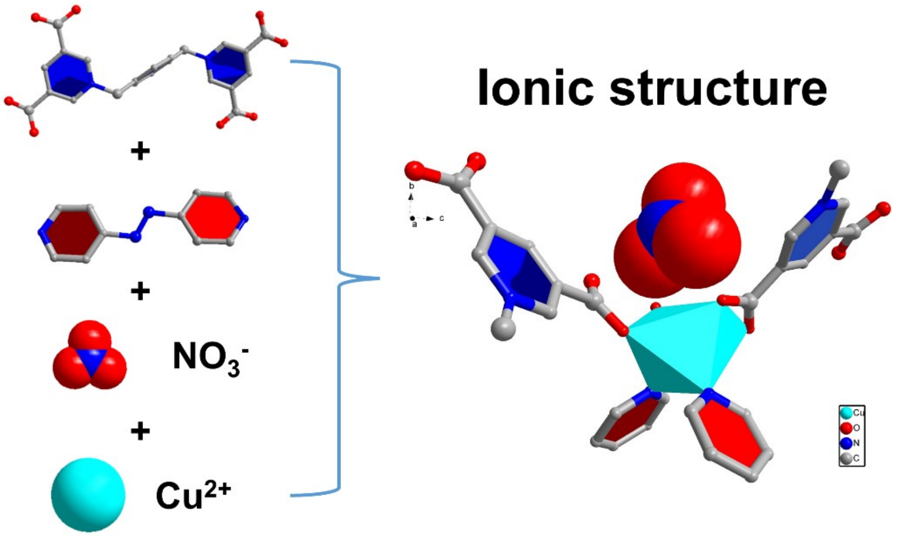

Fig. S1 Chemical structure of ZUT-iMOF-1(Cu).

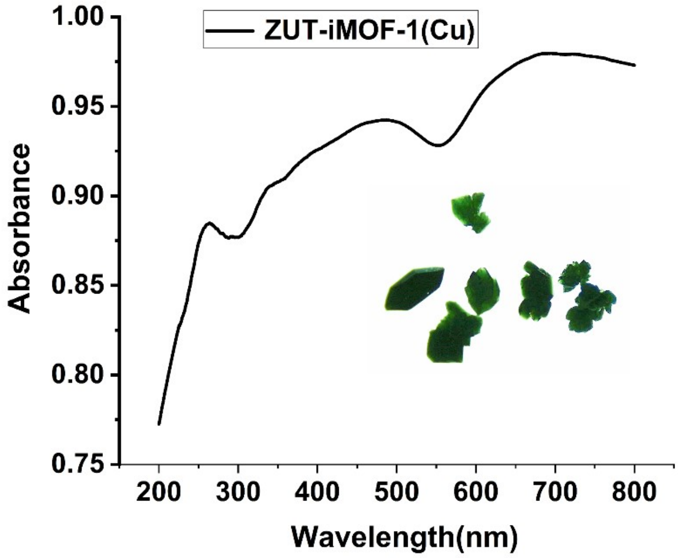

Fig. S2 UV absorption spectra of ZUT-iMOF-1(Cu).

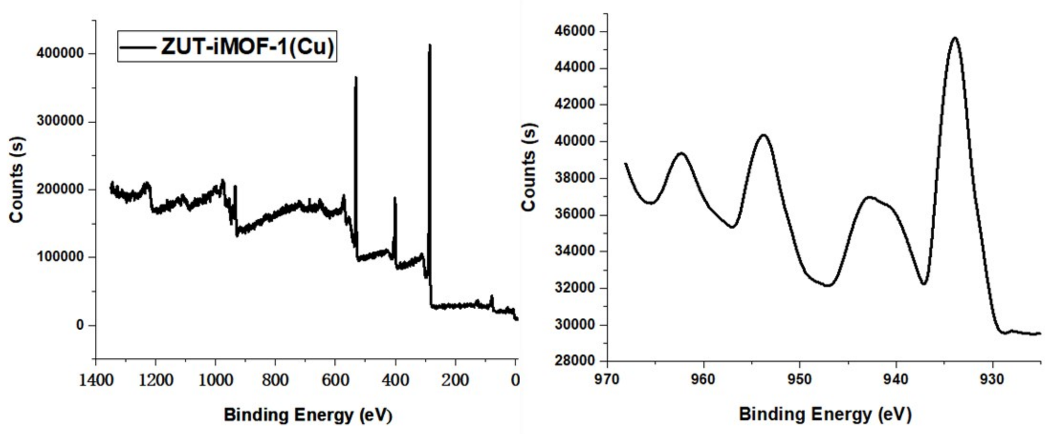

Fig. S3 XPS spectra of ZUT-iMOF-1(Cu).

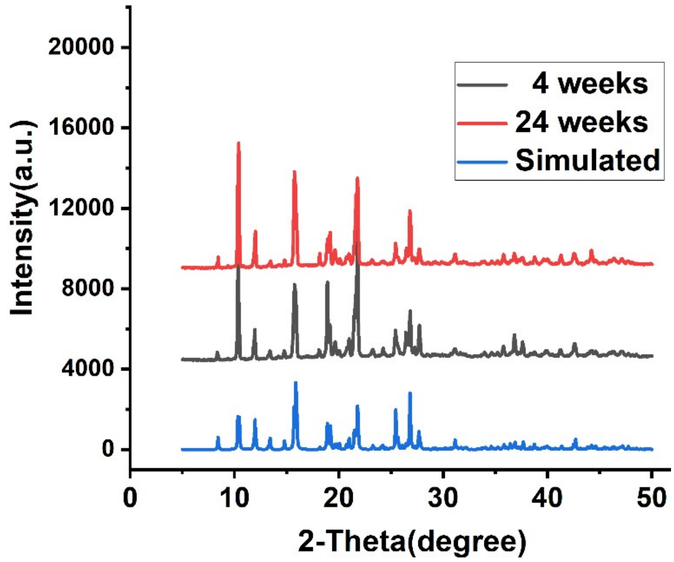

Fig. S4 PXRD spectra of ZUT-iMOF-1(Cu).

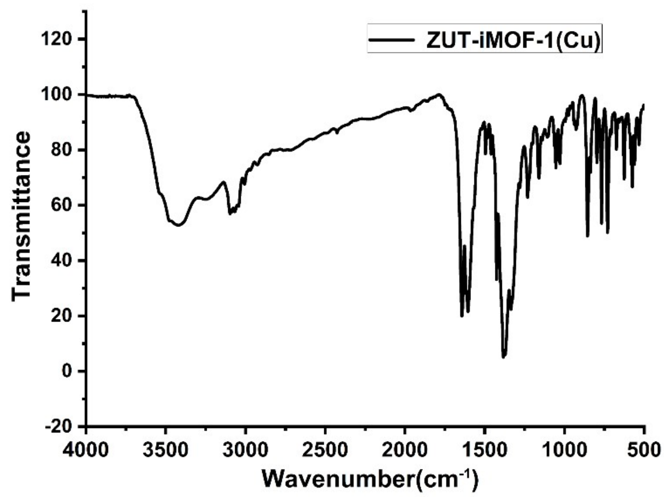

Fig. S5 IR spectra of ZUT-iMOF-1(Cu).

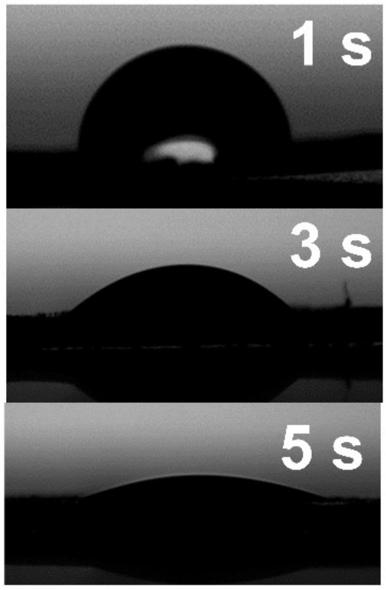

Fig. S6 Water contact angle of ZUT-iMOF-1(Cu).

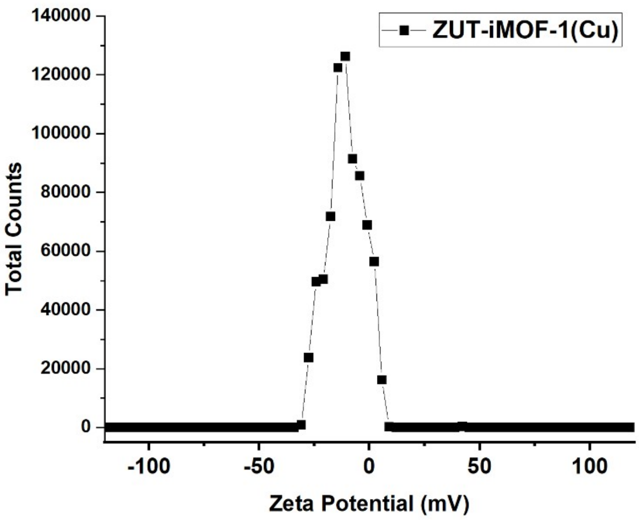

Fig. S7 Zeta potential of ZUT-iMOF-1(Cu).

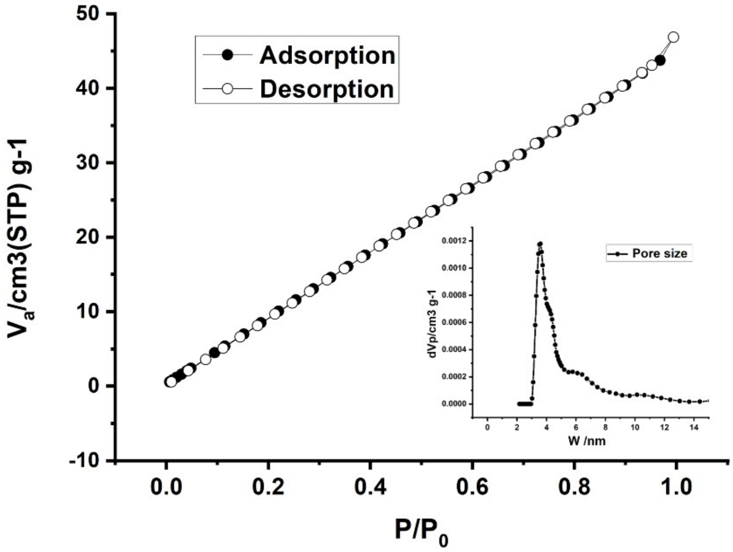

Fig. S8 N_2 adsorption and desorption isotherms of ZUT-iMOF-1(Cu).

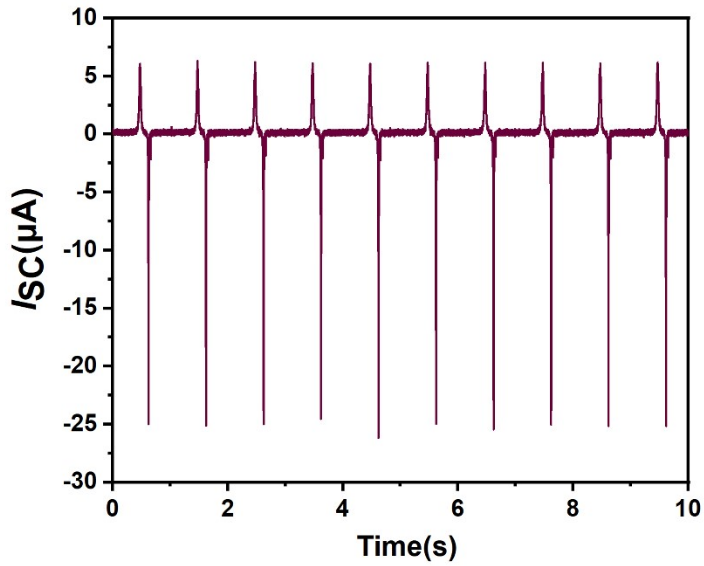

Fig. S9 I_{SC} of iMOF-TENG at 1 Hz.

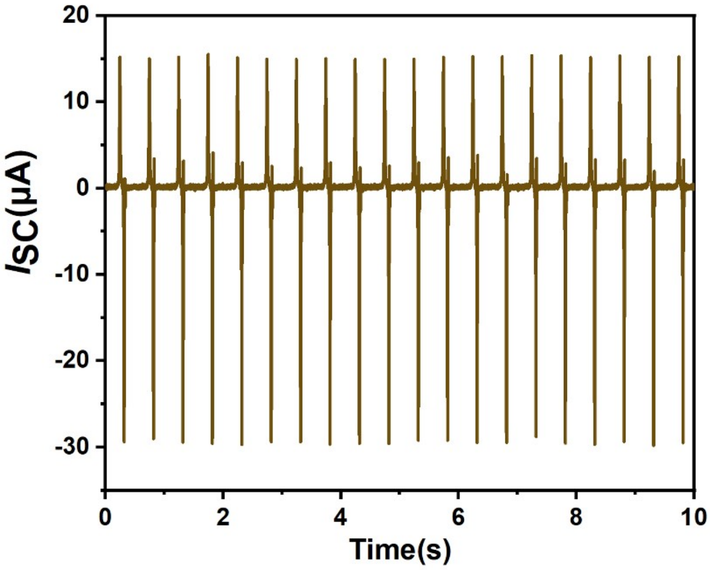

Fig. S10 I_{SC} of iMOF-TENG at 2 Hz.

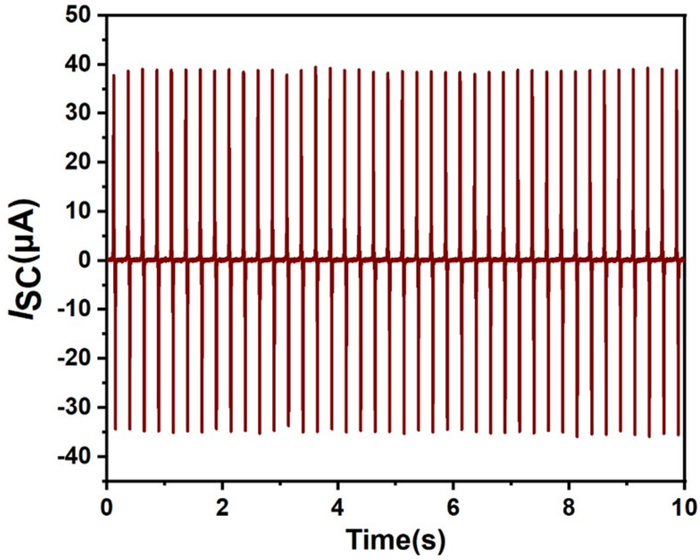

Fig. S11 I_{SC} of iMOF-TENG at 4 Hz.

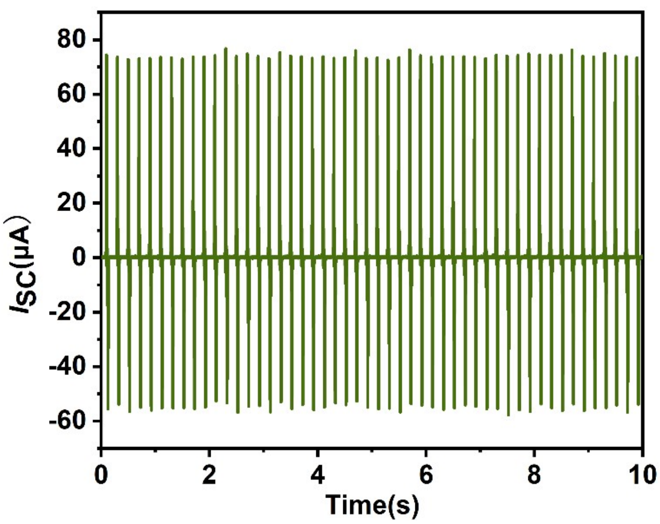

Fig. S12 I_{SC} of iMOF-TENG at 5 Hz.

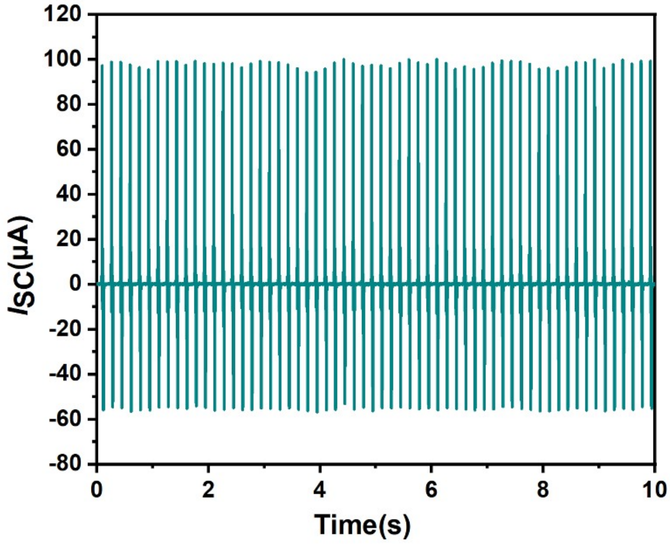

Fig. S13 I_{SC} of iMOF-TENG at 6 Hz.

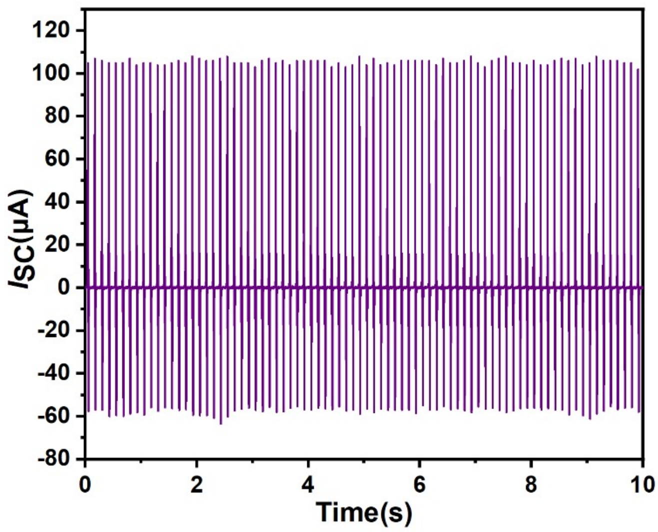

Fig. S14 I_{SC} of iMOF-TENG at 8 Hz.

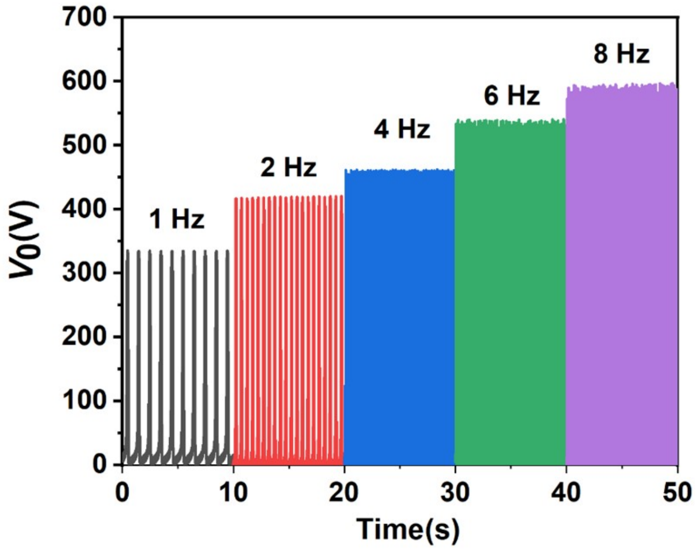

Fig. S15 V_0 of iMOF-TENG from 1 Hz to 8 Hz.

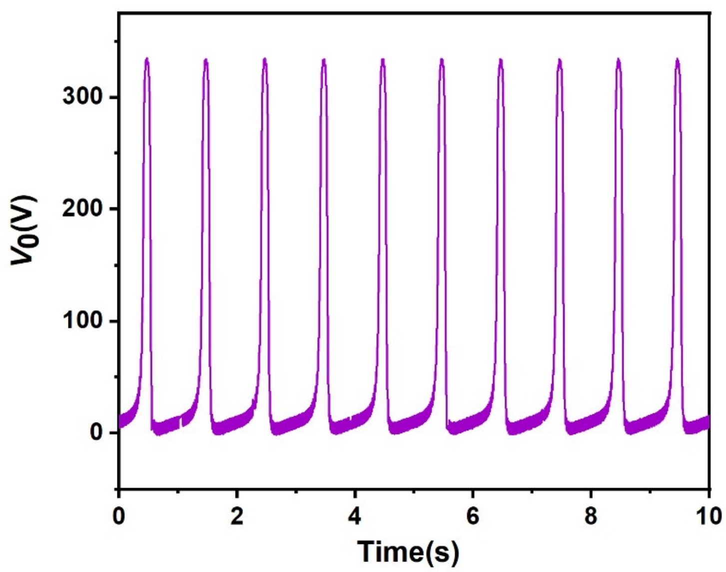

Fig. S16 V_0 of iMOF-TENG at 1 Hz.

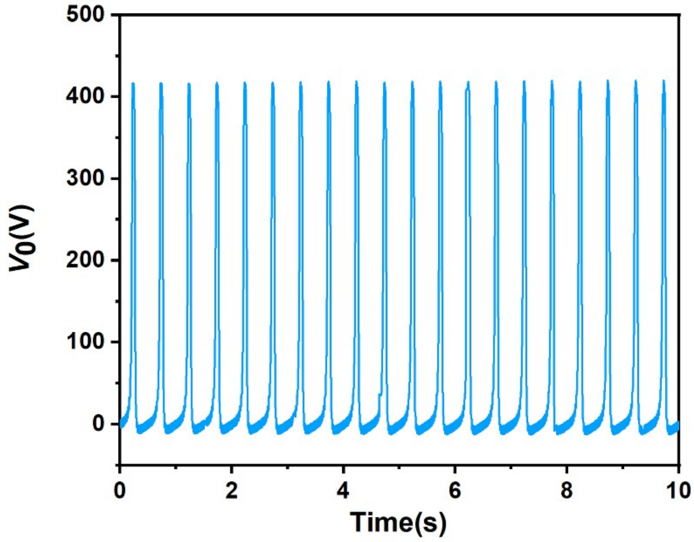

Fig. S17 V_0 of iMOF-TENG at 2 Hz.

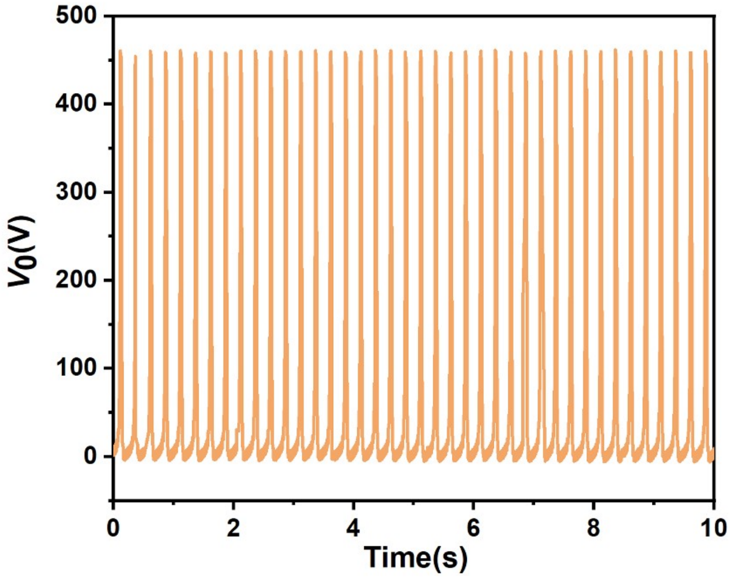

Fig. S18 V_0 of iMOF-TENG at 4 Hz.

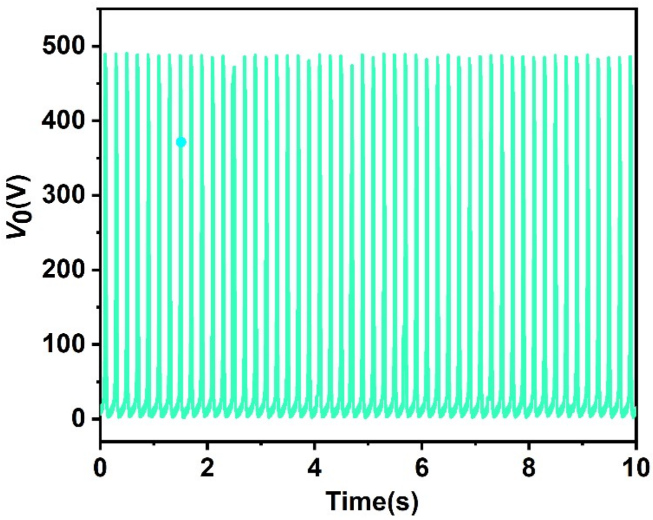

Fig. S19 V_0 of iMOF-TENG at 5 Hz.

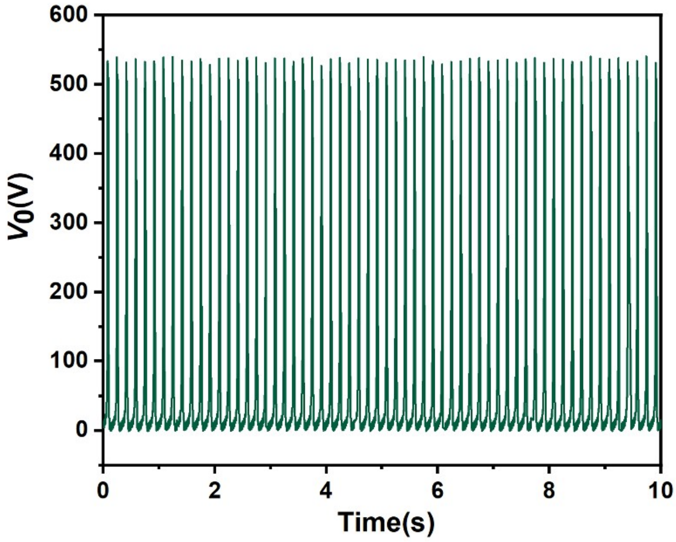

Fig. S20 V_0 of iMOF-TENG at 6 Hz.

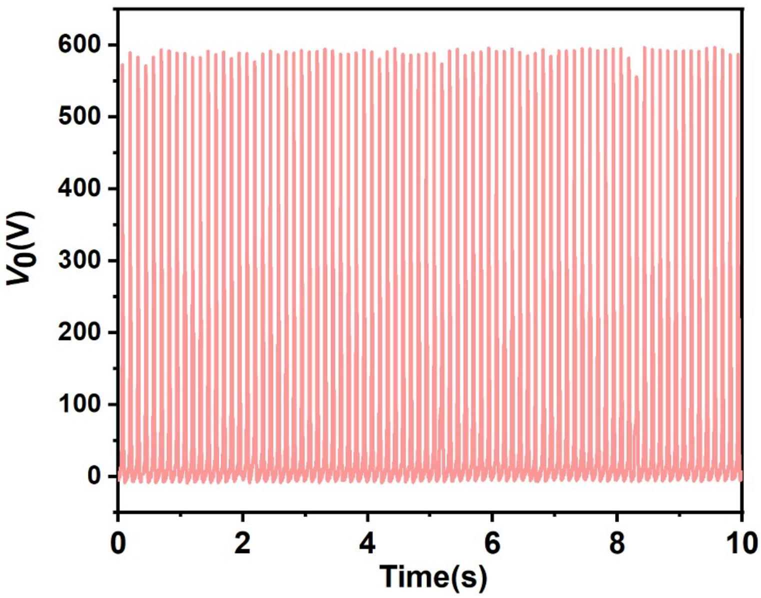

Fig. S21 V_0 of iMOF-TENG at 8 Hz.

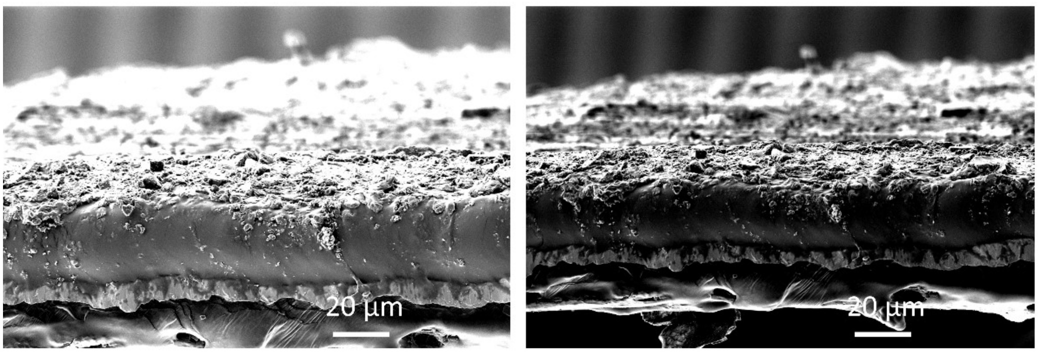

Fig. S22 SEM images of ZUT-iMOF-1(Cu) on the Cu layer (a) before and (b) after testing.

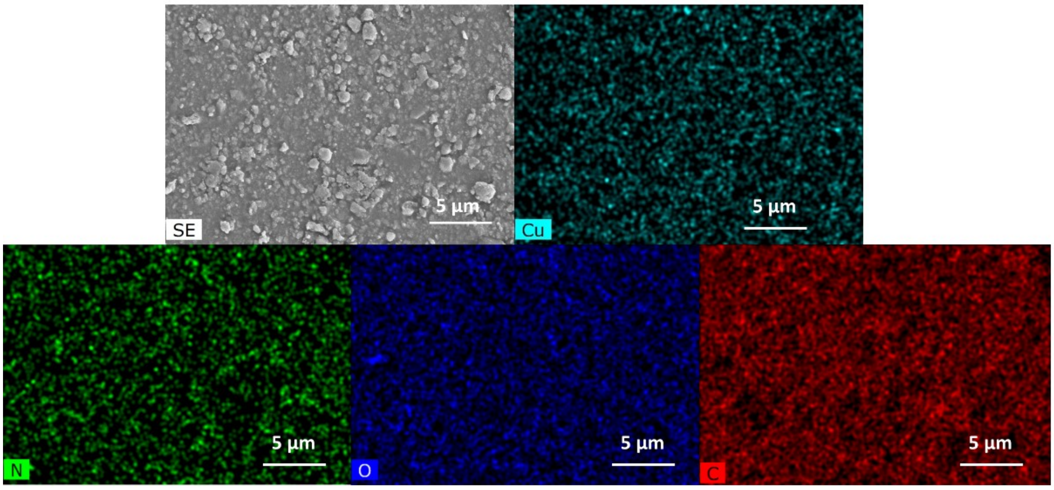

Fig. S23 SEM-EDS mapping analysis image of ground powder of ZUT-iMOF-1(Cu) before testing.

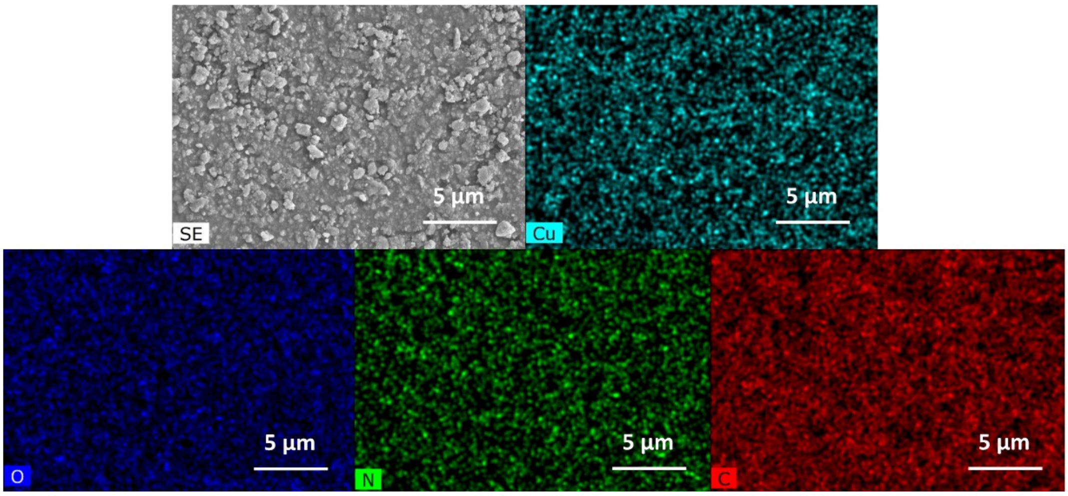

Fig. S24 SEM-EDS mapping analysis image of ground powder of ZUT-iMOF-1(Cu) after testing.

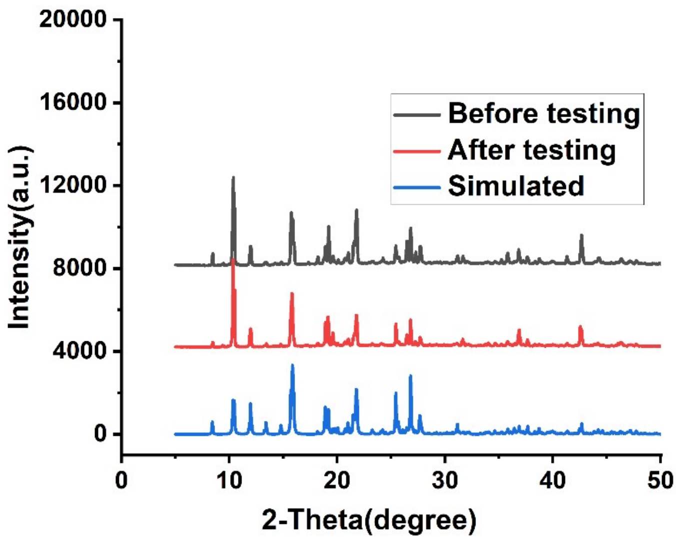

Fig. S25 PXRD spectra of ZUT-iMOF-1(Cu) before and after testing.

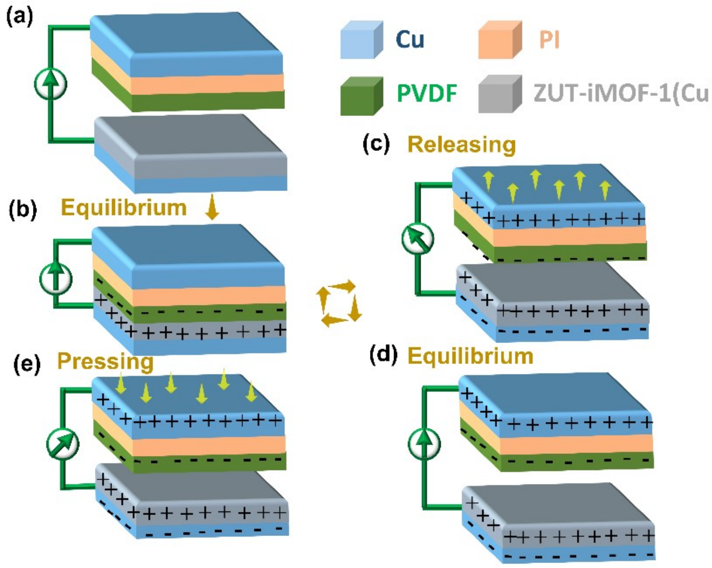

Fig. S26 Working mechanism of TENG based on iMOF-TENG.

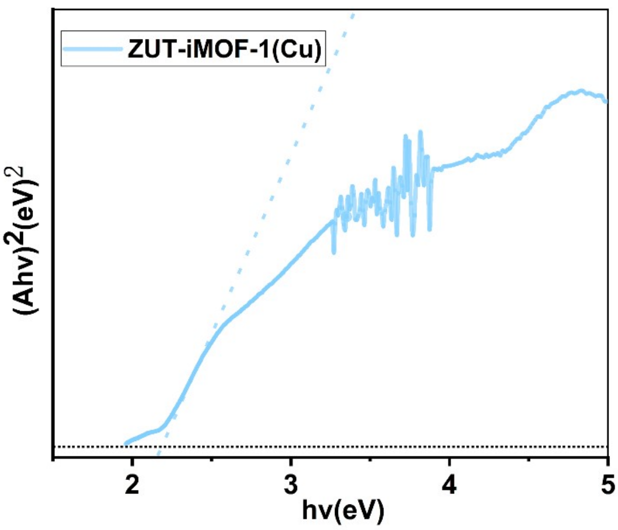

Fig. S27 Tauc plots of ZUT-iMOF-1(Cu).

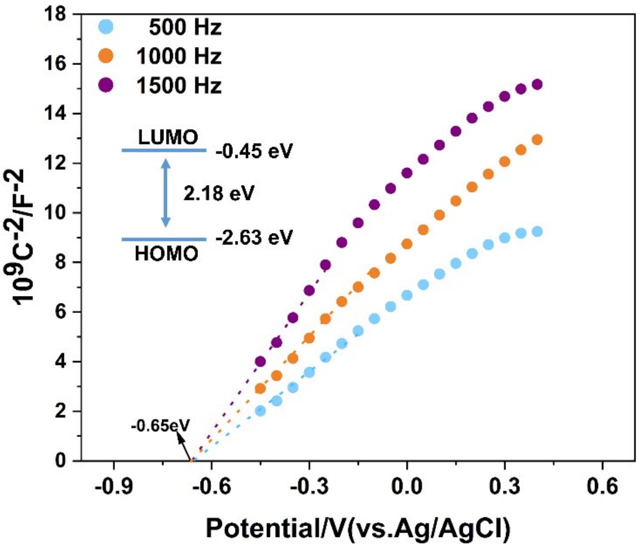

Fig. S28 Mott-Schottky plots of ZUT-iMOF-1(Cu).

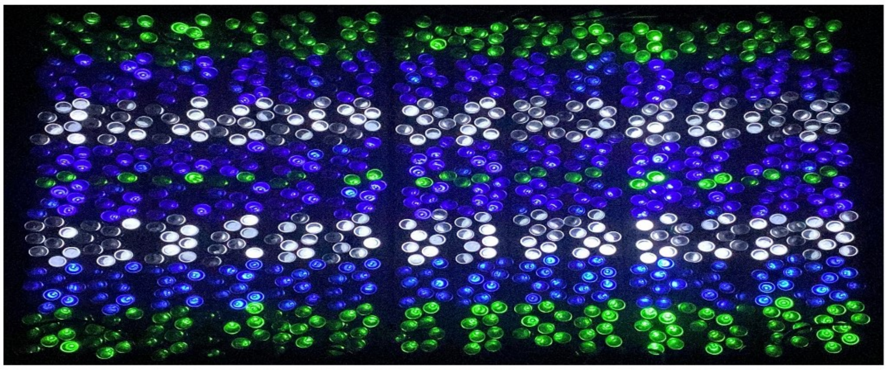

Fig. S29 Commercial LED lights lited by iMOF-TENG.

Table S1 Crystallographic data and structure refinement details for ZUT-iMOF-1(Cu).

Compound	ZUT-iMOF-1(Cu)
Formula	$C_{21}H_{18}CuN_6O_{8.5}$
Mr	553.95
T/K	273.15
l (Mo–Ka)/Å	0.71073
Crystsyst	monoclinic
Space group	$P2_1/n$
a/Å	10.3397(6)
b/Å	14.6943(8)
c/Å	14.9974(8)
α/°	90
β/°	90.685(2)
γ/°	90
Volume/Å^3	2278.5(2)
Z	4
ρ_{calc}(g cm^{-3})	1.615
F(000)	1132.0
μ(mm^{-1})	1.023
R_1 (I >=2σ(I))	0.0375
wR_2 (I > 2σ(I))	0.1070

$R = [\sum||F_0| - |F_c|| / \sum|F_0|]$, $R_W = \sum w[|F_0^2 - Fc^2|^2 / \sum w(|F_w|^2)^2]^{1/2}$

Table S2 Selected bond lengths (Å) and bond angles (deg) for ZUT-iMOF-1(Cu). crystal structure description.

ZUT-iMOF-1(Cu)			
Cu01-O002	1.9801(17)	C00C-C00I	1.379(3)
Cu01-O003	2.0007(18)	C00C-C00N	1.521(3)
Cu01-O0041	2.2238(18)	C00E-C00F	1.508(3)
Cu01-N0082	2.014(2)	C00F-C00H	1.374(3)
Cu01-N009	2.013(2)	C00F-C00I	1.387(3)
O002-C00E	1.268(3)	C00G-C00P	1.512(4)
O004-C00N	1.248(3)	C00G-C00Q	1.389(4)
O003-Cu01-O002	90.51(7)	C00I-C00F-C00E	119.4(2)
O0041-Cu01-O002	99.34(7)	C00I-C00F-C00H	119.0(2)
O0041-Cu01-O003	91.67(7)	C00Q-C00G-C00P	119.7(3)
N0082-Cu01-O002	163.17(8)	C00R-C00G-C00P	121.4(2)
N0082-Cu01-O003	86.37(8)	C00R-C00G-C00Q	118.8(2)
N0082-Cu01-O0041	97.28(8)	C00F-C00H-N006	120.4(2)
N009-Cu01-O002	92.33(8)	C00F-C00I-C00C	120.0(2)
N009-Cu01-O003	172.38(8)	C00O-C00J-N008	123.0(3)
N009-Cu01-O0041	94.83(8)	C00T-C00K-N00A	116.2(3)
N009-Cu01-N0082	88.87(9)	C00U-C00K-N00A	124.7(3)
Symmetry codes:	[1]-1/2+X,3/2-Y,-1/2+Z; [2]1/2+X,1/2-Y,-1/2+Z; [3]1/2+X,3/2-Y,1/2+Z; [4]-1/2+X,1/2-Y,1/2+Z; [5]-X,2-Y,1-Z		

Table S3 Electrochemical parameters of carbon steel obtained from polarization curves with and without TENG.

	E_{corr} (V (*vs*. SCE))	I_{corr} (μA)	$-\beta_c$ (mV dec^{-1})	β_a (mV dec^{-1})
With TENG	-0.755	80.39	188.53	201.04
Without TENG	-0.646	58.28	196.15	198.09

Table S4 Resistance fitting parameters of carbon steel with and without TENG.

	R_s(Ω)	Q		R_{ct}(kΩ)
		Y(s sec^n×10^{-5})	n	
With TENG	554.8	1.608	0.965	18.519
Without TENG	562.2	1.7549	0.911	20.483

Table S5 Output performance comparison of different materials-based TENGs.

Positive materials	Negative materials	Current(I_{sc})	Voltage(V_0)	Ref.
TFP-DP-COF	PVDF	47.9μA	815V	5
Cd-MOF	PVDF	55.32 μA	451.8 V	6
ZIF-62	Teflon/Kapton/Ethyl cellulose	1.4 μA	62 V	46
ZUT-8	PVDF	76.81 μA	562.78 V	24
ZIF-8	Kapton	7 μA	164 V	34
Uio-66	Acrylic Cubstrate	0.3 μA	17.5 V	32
Uio-66-4F	Al	30.6 μA	937.4 V	35
Cu-coated-CFP	PVDF-coated-CFP	7.5 μA	180 V	47
ZnAl	PVDF	5.6 μA	230.6V	48
TPB-DBBA-COF	PVDF	43.6μA	416V	49
ZUT-iMOF-1(Cu)	**PVDF**	**73.79 μA**	**491.45 V**	**This work**